

The key role of decadal modulated oscillation in recent cold phase

Wen Luo¹  | Xiaodan Guan¹  | Yongkun Xie² | Jingchen Liu¹ | Yubin Zhou³ | Beidou Zhang¹

¹Key Laboratory for Semi-Arid Climate Change of the Ministry of Education, College of Atmospheric Sciences, Lanzhou University, Lanzhou, China

²State Key Laboratory of Numerical Modeling for Atmospheric Sciences and Geophysical Fluid Dynamics (LASG), Institute of Atmospheric Physics, Chinese Academy of Sciences, Beijing, China

³National Deep Sea Center, Qingdao, China

Correspondence

Xiaodan Guan, Key Laboratory for Semi-Arid Climate Change of the Ministry of Education, College of Atmospheric Sciences, Lanzhou University, 222# Tianshui South Road, Lanzhou 730000, China.

Email: guanxd@lzu.edu.cn

Funding information

National Science Foundation of China, Grant/Award Numbers: 41521004, 41722502, 41575006, 91637312; China University Research Talents Recruitment Program (111 project), Grant/Award Number: B 13045

Abstract

Global temperature change is strongly affected by internal climate variability (ICV). The temporal change of the ICV on the decadal to multi-decadal scales is referred as the decadal modulated oscillation (DMO) that plays a dominated role in the occurrence of enhanced warming and warming hiatus. However, investigation on the DMO in modern historical period has received limited attention. In this study, the ensemble empirical mode decomposition (EEMD) method was applied to the surface air temperature (SAT) during the boreal cold season to extract the DMO signal in the past century. Two most sensitive areas of DMO trend over northern Eurasia and northwestern North America were identified and used to build a time series of regionally enhanced DMO. It showed an obvious decadal periodic oscillation at 11–23 years and exhibited increasing amplitude. In addition, regression analysis using Niño3.4, Pacific Decadal Oscillation (PDO), Atlantic Multi-decadal Oscillation (AMO), and Arctic Oscillation (AO) revealed a major role of the AO in DMO over the mid-to-high latitudes in the Northern Hemisphere (NH). However, such strong oscillation signal has not been detected in most of the Coupled Model Intercomparison Project Phase 5 (CMIP5) models, and the extracted regionally enhanced DMO are capable of improving the predictability of SAT over the mid-to-high latitudes in the NH.

KEY WORDS

Arctic Oscillation, CMIP5, decadal modulated oscillation, internal climate variability

1 | INTRODUCTION

The carbon dioxide in the atmosphere has increased monotonically over the past century (Stocker *et al.*, 2013) and is considered to be responsible for global warming. However, global mean surface air temperature (SAT) did not rise significantly since the late 1990s, which contradicted the global warming theory based on greenhouse gas increase (Stocker *et al.*, 2013; Steinman *et al.*, 2015; Huang *et al.*, 2016; Guan *et al.*, 2017; Liu and Zhou, 2017). This decadal signal of cooling phenomenon drew the attention of the public (Easterling and Wehner, 2009; Kaufmann *et al.*, 2011; Li *et al.*, 2015), and was named global warming hiatus (Fyfe *et al.*, 2013).

So far, numerous studies have explored the mechanisms of the warming hiatus and revealed it is strongly correlated with the internal climate variability (ICV; Kosaka and Xie, 2013; Dai *et al.*, 2015; Guan *et al.*, 2015a; Fyfe *et al.*, 2016; Huang *et al.*, 2016; Meehl *et al.*, 2016; Liu and Zhou, 2017), such as the Inter-decadal Pacific Oscillation (L'Heureux *et al.*, 2013; Dai *et al.*, 2015; Meehl *et al.*, 2016), the cooling of the La Niña-like event (Kosaka and Xie, 2013), the negative phase of the North Atlantic Oscillation (NAO; Higuchi *et al.*, 1999; Huang *et al.*, 2006; Luo *et al.*, 2015), and the neutral Atlantic Multi-decadal Oscillation (AMO; Wyatt *et al.*, 2012; Tung and Zhou, 2013). On the other hand, from the view of energy balance, a few studies indicated that heat was stored in the deeper Atlantic

Ocean and southern oceans during the warming hiatus (Chen and Tung, 2014; 2016; Xie *et al.*, 2017).

To better understand global climate change, an increasing number of scholars have explored the SAT change over the past hundred years on global and regional scales (Huang and Liu, 2000; Hansen *et al.*, 2006; Zhang *et al.*, 2011; Li *et al.*, 2012). However, most of these studies used traditional statistical methods to analyse temperature variability, such as simple linear fitting based on least squares estimator that calculates the variation trend only at a constant rate. It is generally accepted that the temperature change is nonlinear and non-stationary (Huang *et al.*, 1998; Wu *et al.*, 2007; Chen *et al.*, 2016). Traditional statistical method such as time-unvarying linear trend cannot effectively reveal the potential features of temperature variability (Ji *et al.*, 2014).

Actually, other methods exist, which can avoid the shortcoming of linear methods to show non-stationary and nonlinear characteristics of the data, such as the ensemble empirical mode decomposition (EEMD) method that proposed by Wu and Huang (2009). The effectiveness of EEMD is based on improvement of the traditional empirical mode decomposition (EMD) method (Huang *et al.*, 1998) and has been gradually applied extensively in climate and oceans studies (Qian *et al.*, 2009; 2011a; Bai *et al.*, 2014; Ji *et al.*, 2014; Zhang *et al.*, 2016; Li *et al.*, 2017; Shan *et al.*, 2017). For example, Qian *et al.* (2011a) studied the multi-timescale variability of SAT in China; Zhang *et al.* (2016) analysed aerosol trends and rates of change; Li *et al.* (2017) presented extensive tests from several different aspects to validate the effectiveness of predicting the sea surface temperature; and Shan *et al.* (2017) investigated the modulated annual cycle (MAC) of the Indo-Pacific warm pool (IPWP) heat centre location, all using the EEMD method.

Recently, Huang *et al.* (2016) extracted the oscillation components of ICV on the decadal to multi-decadal scales and referred it as the decadal modulated oscillation (DMO). The term of DMO denotes the modulation effects of oceanic ICV modes and Arctic on the SAT change at decadal to multi-decadal time scales. It affects the SAT through changing the asymmetric meridional and zonal thermal forcing (MTF and ZTF, respectively; Huang *et al.*, 2016; Guan *et al.*, 2017). However, some important aspects of the DMO are still unclear, such as how the DMO changed in the past 115 years (1901–2015) and its effect on climate change. In this study, we utilized the EEMD method to extract the DMO signal of SAT and built a regionally enhanced DMO based on sensitive areas to analyse its long-term periodic variation. This paper is arranged as follows. The details of the data sets and the methodology used are given in section 2. Our findings are provided in section 3, and conclusions and discussions are presented in section 4.

2 | DATA AND METHODS

2.1 | Data sources

In this study, we used monthly mean SAT data from the Climatic Research Unit (CRU) time series data set (version 4.01), provided by the University of East Anglia (Harris *et al.*, 2014), to investigate the temperature change during the cold season (November to the following March). The data set covers the period from 1901 to 2016 with a high spatial resolution of $0.5 \times 0.5^\circ$. In addition, to explore the atmospheric circulation effects on the DMO, we selected four classic climate indexes of Niño3.4, Pacific Decadal Oscillation (PDO), AMO, and Arctic Oscillation (AO), which were downloaded from the Climate Explorer (<http://climexp.knmi.nl/>).

To assess the performances of climate models in simulating DMO, we used outputs from the Coupled Model Intercomparison Project Phase 5 (CMIP5) models. The CMIP5 experiments (Taylor *et al.*, 2011) include simulations of 20th-century climate (referred as historical experiments) and of 21st-century climate under new greenhouse gas emission scenarios (referred as representative concentration pathways [RCPs]; Meinshausen *et al.*, 2011). The RCPs represent different emission pathways according to assumed policy decisions, which would influence the future emissions of greenhouse gases, aerosols, ozone, and land-use changes (Bannister *et al.*, 2017). In this study, the outputs for temperature from the historical simulations of 19 models were selected (Table 1), together with their RCP4.5 outputs runs from 2005 to 2015, to compare with the observational data set. In order to be consistent with the observational data set, all model outputs were interpolated onto the $0.5 \times 0.5^\circ$ grid, and the temperature anomalies in models were calculated with respect to the mean from 1961 to 1990.

2.2 | Methods

The EEMD method is applied to decompose the time series of SAT in this study. It is a new time series signal processing method, and suitable for non-stationary and nonlinear signal detection, which can decompose the original signal into oscillations at different time scales (intrinsic mode function [IMF]) and the trend component (Wu and Huang, 2009; Chen *et al.*, 2016). In the calculation process of using EEMD method, the noise added to data has an amplitude that is 0.2 times the standard deviation of the raw data, and the ensemble number is 400. Considering that the EEMD method has an end effect (Qian *et al.*, 2011b), we need to eliminate the minor influence of end effect on our results, the first and last years of all the decomposed results are excluded. Moreover, the temperature data from the CRU used in this study cover the period from 1901 to 2015; the

TABLE 1 Summary of CMIP5 models used in this study

Model name	Modelling centre
CanESM2	Canadian Centre for Climate, Canada
CCSM4	National Center for Atmospheric Research, United States
CNRM-CM5	Centre National de Recherches Meteorologiques, France
CSIRO-Mk3.6	Commonwealth Scientific and Industrial Research, Australia
GFDL-CM3	Geophysical Fluid Dynamics Laboratory, United States
GFDL-ESM2G	Geophysical Fluid Dynamics Laboratory, United States
GFDL-ESM2M	Geophysical Fluid Dynamics Laboratory, United States
GISS-E2-R	NASA Goddard Institute for Space Studies, United States
HadGEM2-CC	Met Office Hadley Centre, UK
HadGEM2-ES	Met Office Hadley Centre, UK
INM-CM4	Institute for Numerical Mathematics, Russia
IPSL-CM5A-LR	Institute Pierre-Simon Laplace, France
IPSL-CM5A-MR	Institute Pierre-Simon Laplace, France
MIROC5	Atmosphere and Ocean Research Institute, Japan
MIROC-ESM	Japan Agency for Marine-Earth Science and Technology, Japan
MIROC-ESM-CHEM	Japan Agency for Marine-Earth Science and Technology, Japan
MPI-ESM-LR	Max Planck Institute for Meteorology, Germany
MRI-CGCM3	Meteorological Research Institute, Japan
NorESM1-M	Norwegian Climate Centre, Norway

Note. Both historical runs for the period 1901–2005 and future scenario RCP4.5 runs from 2006 to 2015 are used.

first and last years of all the decomposed results via the EEMD method are excluded, leaving the period of 1902–2014 for further analysis.

Note that the “trend” used in this paper refers to the linear trend over a specific period, which is calculated by the least squares method and may not refer to the long-term trend. The “long-term trend” in this paper refers to the linear trend over past 115 years from 1901 to 2015.

3 | RESULTS

According to the IPCC AR5, during the global warming over past 100 years, the temperature during cold season

exhibited the largest warming trend when compared to that during the other seasons, and also showed a more obvious cooling trend in recent decades when compared with that during warm season (Huang *et al.*, 2016). The temperature variability in the cold season is more closely associated with atmospheric circulation than that in summer. Thus, further research on the SAT change during the boreal cold season is needed. We first calculated the time series of SAT anomaly in terms of the cold season from 1901 to 2015 over the NH land (Figure 1). It shows a distinct downtrend during 2001–2013, which was much different from the enhanced warming in the previous decade. Hitherto, the dominant mechanism that has been proposed to understand the temperature variability, is the effects of ICV, which has been increasingly investigated in recent years (Crétat *et al.*, 2011; Crétat and Pohl, 2012). Huang *et al.* (2016) extracted the ICV of SAT on the decadal to multi-decadal time scales in the cold season and proposed that the cooling phase of ICV was responsible for the warming hiatus (Guan *et al.*, 2017).

To verify the effect of ICV on temperature change over the NH land, we applied the EEMD method to decompose the time series of SAT anomaly in the cold season over the NH land during 1901–2015, and obtained five IMF components (C_{1-5}) and long-term trend (R) (Figure 2; Wu *et al.*, 2011; Ji *et al.*, 2014). The five IMF components reflect the fluctuation characteristics from high to low frequency at different time scales, which are thought to be induced mainly by the ICV (Wu *et al.*, 2011; Wallace *et al.*, 2012; Smoliak *et al.*, 2015; Guan *et al.*, 2015a). The oscillation cycles of C_1 and C_2 are about 3 and 7 years, respectively. The oscillation cycles of C_3 , C_4 , and C_5 are about 14, 20, and 70 years, respectively. The long-term trend is closely associated with radiative forcing (Wu *et al.*, 2011; Guan *et al.*, 2015b).

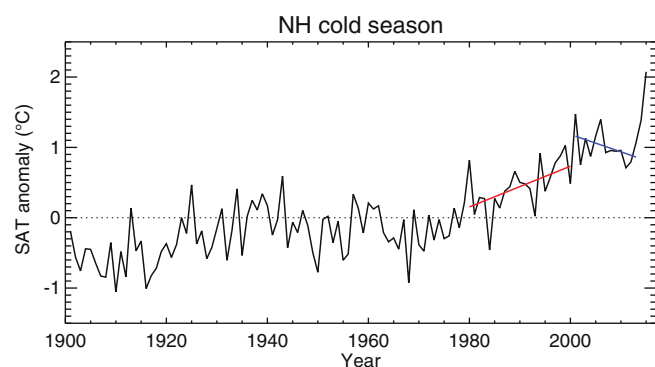


FIGURE 1 Regional-mean time series of SAT anomaly relative to 1961–1990 over the Northern Hemisphere land for the cold season. The red line is the linear trend for 1980–2000; and the blue line for 2001–2013. Note that the boreal cold season spans from November to the following March [Colour figure can be viewed at wileyonlinelibrary.com]

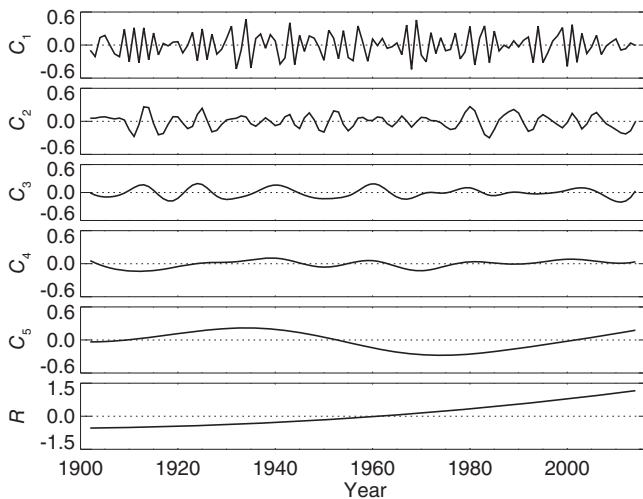


FIGURE 2 EEMD decomposition of the time series of mean SAT anomaly in the cold season over the NH land. C_1 – C_5 represent five IMFs from high to low frequency, while R represents the long-term trend

According to the IMF components of different oscillation cycles, we reconstructed the inter-annual variability, inter-decadal variability, and the long-term trend of the SAT anomalies. The inter-annual temperature variability was obtained by using the sum of IMFs C_1 and C_2 ; the inter-decadal temperature variability by using the sum of IMFs C_3 , C_4 , and C_5 ; and the long-term trend is the residual (R). As illustrated in Figure 3, compared with the original temperature anomaly, the reconstructed inter-annual temperature variability represents the fluctuation of high-frequency signals, and the reconstructed inter-decadal temperature variability fully reflects the overall trend of the temperature variability on the decadal to multi-decadal time scales from 1902 to 2014. Since the amplitude of the inter-decadal temperature variability is comparable to that of the long-term trend on the decadal to multi-decadal time scales, the inter-decadal temperature variability enhances or suppresses the

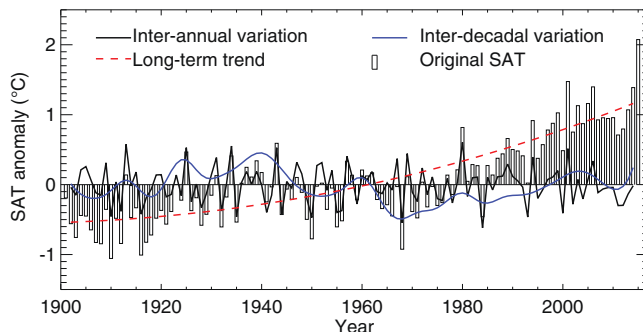


FIGURE 3 EEMD-decomposed raw SAT anomalies (bar) for the long-term trend component (red dashed line), inter-decadal component (blue curve), and the inter-annual component (black curve) [Colour figure can be viewed at wileyonlinelibrary.com]

long-term trend at the decadal time scale. For instance, during the accelerated warming period in 1985–1998, the inter-decadal temperature variability was in an upwards phase and enhanced the uptrend of the long-term trend. On the contrary, when the inter-decadal temperature variability was in a downwards phase since 2000, it balanced or reduced the radiatively forced warming (the long-term trend; Guan *et al.*, 2015b) and resulted in the warming hiatus over the NH land. Based on the above analysis, we conclude that the sum of IMFs C_3 , C_4 , and C_5 can represent the inter-decadal variability of SAT over the NH land, and it is defined as the DMO following Huang *et al.* (2016). In the remainder of this paper, we extract the DMO signal from raw SAT in the same way.

Figure 4 compares spatial maps of DMO (Figure 4a) and SAT trends (Figure 4b) in boreal cold season in response to the warming hiatus. Most areas experienced a decreased trend of DMO, and two obvious decreasing centres where the DMO trend was less than -2°C for 13 years were located in northern Eurasia (Kazakhstan, northwestern Russia, and northeastern China) and northwestern North America (western Canada and Alaska). Meanwhile, it shows small positive trend over northeastern Russia, eastern United States, eastern Canada, and Greenland. Compared with Figure 4a, the spatial distribution of SAT trend (Figure 4b) exhibits a similar pattern as that of DMO, with a smaller amplification in most of the downwards trend areas, such as Russia and North America. Positive trend of SAT was observed in northern Africa and western Europe, and the uptrend was remarkably stronger than that of DMO, which was induced by strong local warming effect from radiative factors (Guan *et al.*, 2015b; Zhang *et al.*, 2017). Based on the above, we analysed the effects of DMO on SAT from two sides, the temporal evolution and spatial distribution. Results demonstrate that DMO dominated the SAT variation over the past century, especially during the recent warming hiatus period.

Because of the key role of DMO in temperature change, we further explored the long-term variation of DMO in the past century. Figure 4a indicates that most areas experienced a decreasing trend of DMO in the NH during the warming hiatus period. In particular, two obvious decreasing centres located in northern Eurasia (Kazakhstan, northwestern Russia, and northeast China) and northwestern North America (western Canada and Alaska) made the largest contribution to the cooling over the NH. Based on these two major contribution areas, we built a time series of regionally enhanced DMO to explore the long-term variation of DMO in the past century.

Figure 5 shows a time series of regionally enhanced DMO from 1902 to 2014, it appears a strong decadal variability with periodic oscillation around 11–23 years. The

FIGURE 4 Spatial distribution of the linear trend for 2001–2013 in the boreal cold season of the (a) DMO and (b) SAT [Colour figure can be viewed at wileyonlinelibrary.com]

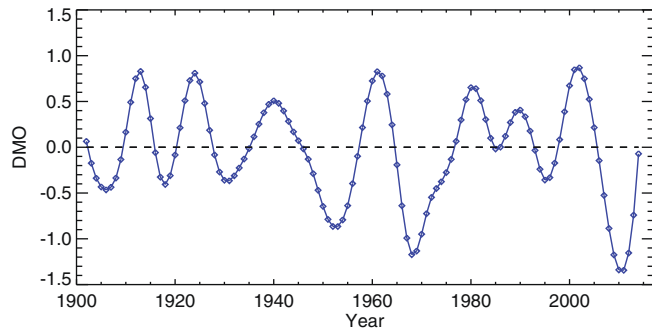
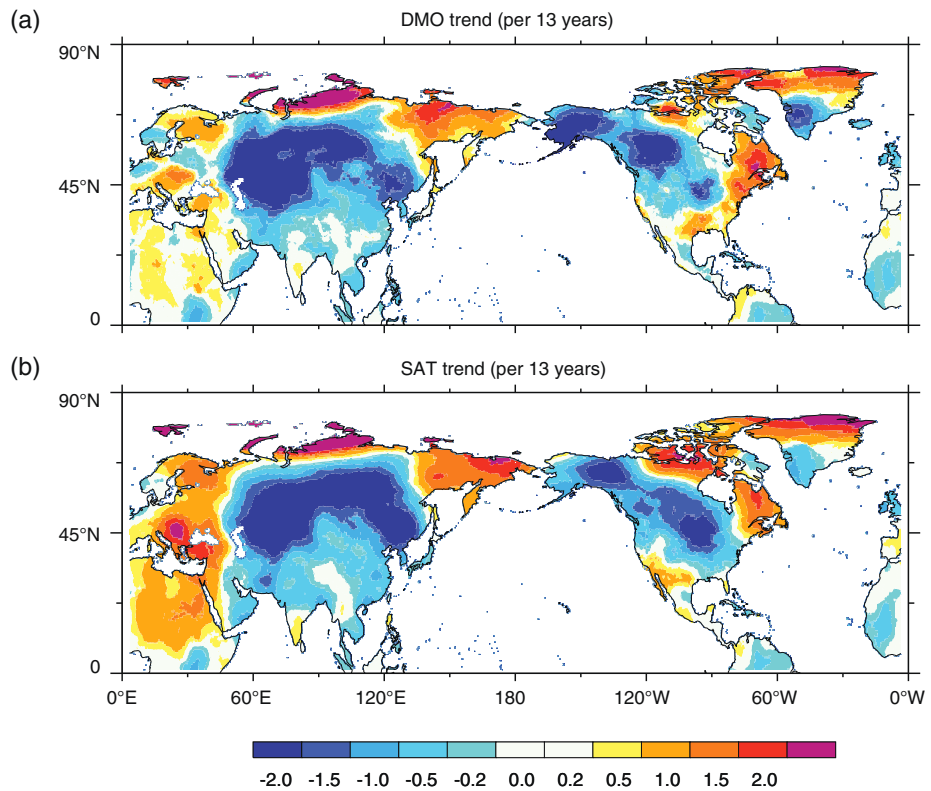


FIGURE 5 Time series of regionally enhanced DMO during 1902–2014 based on two most significant downwards trend areas of northern Eurasia and northwestern North America [Colour figure can be viewed at wileyonlinelibrary.com]

peak values were stable about 0.9°C , and the trough values gradually decreased from -0.5 to -1.4°C , which implied an intensified oscillation. During the accelerated warming period of 1980–2000, DMO had a notably bigger trough value than in both the previous cycle (before 1980) and the following cycle (after 2000), which was only down to about 0°C . It indicated that DMO's downtrend was not enough to offset the warming effect of greenhouse gases, which became an additional contribution to the accelerated warming. During 2000–2011, the DMO rapidly dropped from peak to trough, which contributed to the warming hiatus. Beginning in 2012, the DMO reversed. It is striking to

see that the rising of DMO during 2012–2014 was faster than any uptrend since 1902. These characteristics indicate that DMO arrived at new peaks of both negative and positive phases, causing an intensified oscillation on the decadal time scale.

Since the DMO change is strongly linked to global-scale climate variability, we further explored the modulated effects of oceanic ICV on DMO. Four classic climate indexes (PDO, AMO, Niño3.4, and AO) were selected to regress the time series of regionally enhanced DMO during 1950–2014. First, we applied the EEMD method to decompose each index and obtain six IMFs, respectively. Then, we selected IMFs 3, 4 and 5 of each index to regress the regionally enhanced DMO by using the stepwise multiple linear regression (MLR) method. The regressed regionally enhanced DMO shown in Figure 6 can be expressed as follows:

$$\begin{aligned} \text{DMO} = & -0.29 + 1.26\text{PDO}_4 + 3.12\text{AMO}_3 + 0.74\text{Ni}\tilde{\text{o}}3.4_4 \\ & + 1.68\text{Ni}\tilde{\text{o}}3.4_5 + 1.46\text{AO}_3 - 2.09\text{AO}_4 + 2.11\text{AO}_5. \end{aligned}$$

The regression-based approximation of DMO component can explain 80% of its variance using classic oceanic ICV modes: PDO, AMO, Niño3.4, and AO with contributions of 14, 4, 16, and 66%, respectively. Figure 6 compares the time series of the regressed DMO with the observed regionally enhanced DMO. It is found that the regressed DMO captures

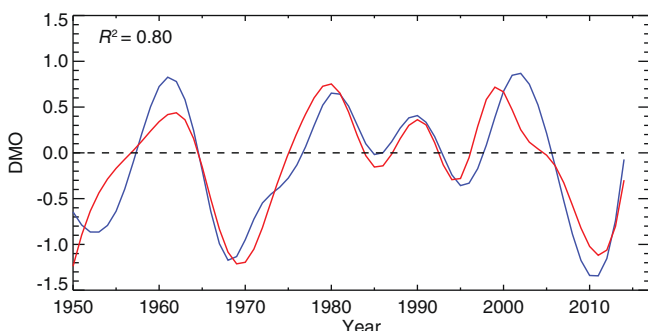


FIGURE 6 Time series of regionally enhanced DMO component (blue), and regressed DMO using the decadal variability of the PDO, AMO, Niño3.4, and AO indexes (red) [Colour figure can be viewed at wileyonlinelibrary.com]

the major variation features of the observed regionally enhanced DMO, with the largest contribution from the AO.

Numerous studies have shown that the AO plays an essential role in climate change over mid-to-high latitudes of the NH on inter-annual to decadal time scales (Thompson and Wallace, 1998; 2001; Gong and Ho, 2003). Thompson and Wallace (2001) pointed out that the AO signal is strongly coupled to SAT over the Eurasian continent in winter. Gong and Wang (2003) demonstrated that the significant relationship between the AO and precipitation in winter over China. The AO signal is closely related to lower tropospheric circulations, such as the East Asian winter monsoon, the Aleutian Low, and the Siberian High (Gong *et al.*, 2001; Wu and Wang, 2002). In addition, the AO also showed marked impacts on extreme weather events (Thompson and Wallace, 2001; Wettstein and Mearns, 2002; Mao *et al.*, 2011), including blocking and cold air activities in the NH (Thompson and Wallace, 2001), extreme temperatures in northeastern United States and in Canada (Wettstein and Mearns, 2002).

In the last few decades, the Arctic region experienced an enhanced and accelerated warming (Serreze *et al.*, 2009), which is termed as the Arctic amplification (AA; Holland and Bitz, 2003). A number of studies suggested that the AA effect of the Arctic region has been highly correlated to frequent extreme weather events across the mid-latitudes in the NH (Overland and Wang, 2010; Hopsch *et al.*, 2012). Three potential dynamical pathways linking the AA to mid-latitude weathers have been revealed, including changes in storm tracks, the jet stream, and planetary waves along with their associated energy propagation (Cohen *et al.*, 2014).

Besides the AO effect, the recent warming hiatus was also influenced by decadal variability in the Pacific Ocean (Kosaka and Xie, 2013; Dai *et al.*, 2015). Kosaka and Xie (2013) pointed out that the classic Pacific variability related to the recent warming hiatus was mainly the La Niña-like cooling induced by accelerated trade winds. Dai *et al.*

(2015) concluded that the Inter-decadal Pacific Oscillation (IPO) was largely responsible for the recent slowdown of warming. However, such influence from the Pacific Ocean is limited to the North America generally.

Considering that the global climate models are useful tools for investigating climate change, we utilized the CMIP5 models to reveal the key role of DMO in SAT. Note that multi-model ensemble strategy is traditionally used to exploit the diversity of skilful predictions by different models (Xu and Xu, 2012; Zhang, 2012), but this method does not consider the relative strength and weakness of each model as an ensemble invariably hides the substantial variation among individual models (Bannister *et al.*, 2017). In addition, the internal variability of different models might be offset or strengthened through ensemble mean. Consequently, we focused on intercomparison between individual models and their individual merits in this study.

The outputs of 19 CMIP5 models were used to generate time series of regionally enhanced DMO based on the two most sensitive areas observed over northern Eurasia and northwestern North America, as shown in Figure 7. There are large differences in phase variation and amplitude among simulated DMO signals. Correlation coefficients between simulated and observed DMO are given in Figure 8. Only four out of the 19 models showed a significant relationship and passed the 99% confidence level, in which only CSIRO-Mk3.6 (0.28) and HadGEM2-ES (0.28) have positive correlations while HadGEM2-CC and INM-CM4 reveal significant negative correlations.

Given the closest DMO in CSIRO-Mk3.6 and HadGEM2-ES simulations to the observation, we compared the observed area-average SAT in two most sensitive areas (i.e., northern Eurasia and northwestern North America) with simulated area-average SAT of the above two models (Figure 9a). The observed SAT exhibited a clear increase from 1950 until the early 1960s, but it decreased during the period 1960–1970. In addition, there was a continuous rise in SAT from 1970 until 2000, which reached a new level of about 1°C higher. Thereafter, the SAT started a new oscillation with a smaller amplitude and shorter cycle than those before 1980. However, the simulated SAT of the two models exhibits a rather flat change, which shows that the simulated time series are considerably smoother than the observed SAT curve. Both models simulated the opposite trend during 1950–1970 compared to the observed SAT trend. Beginning in 1970, although the simulated SAT showed an increase, the uptrend was smaller than that of the observed SAT. During the warming hiatus, HadGEM2-ES simulated a larger downtrend than the observed SAT, while CSIRO-Mk3.6 still simulated an increase in SAT. Therefore, we conclude that these models cannot capture the basic phase variation and amplitude of the observed SAT.

FIGURE 7 Time series of the observed DMO (black) and simulated DMO by the CMIP5 models [Colour figure can be viewed at wileyonlinelibrary.com]

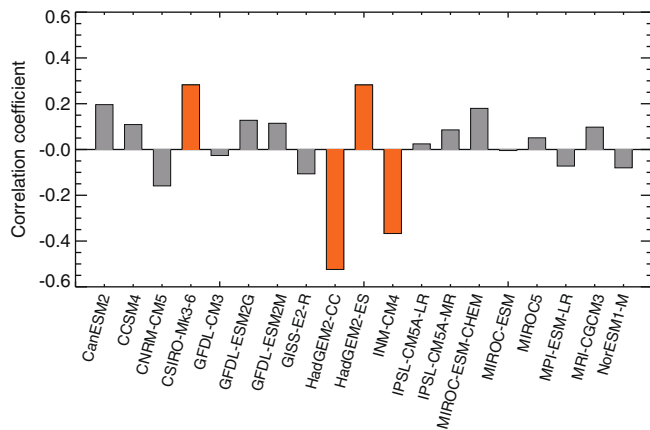
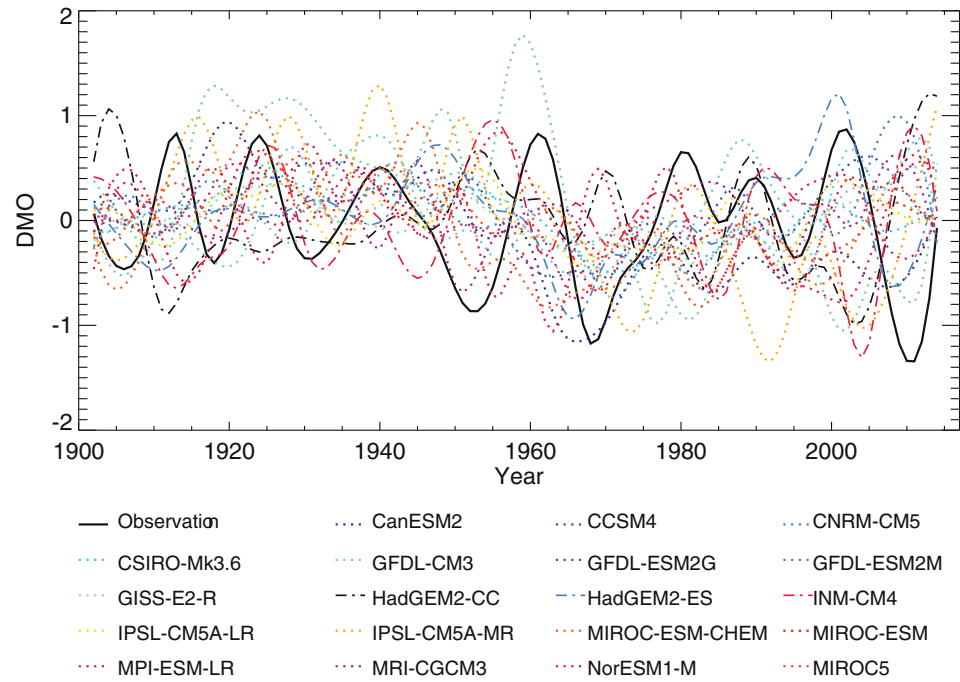


FIGURE 8 Correlation coefficients between the observed and simulated DMOs. Correlation coefficients that pass the 99% confidence level are given in orange [Colour figure can be viewed at wileyonlinelibrary.com]

Once we replaced the simulated DMO with the observed regionally enhanced DMO and added it to the simulated C_1 , C_2 , and R to obtain the “hybrid” SAT, as shown in Figure 9b, the improvement of the “hybrid” SAT becomes obvious: the phase variation on the decadal time scale and the amplitude of the “hybrid” SAT are broadly comparable to the observations. In addition, CSIRO-Mk3.6 shows an amplitude that is closer to the observation than HadGEM2-ES, especially after the late 1970s. That is to say, CSIRO-Mk3.6 has a better performance than HadGEM2-ES. According to previous regression analysis (Figure 6), the regionally enhanced DMO can be

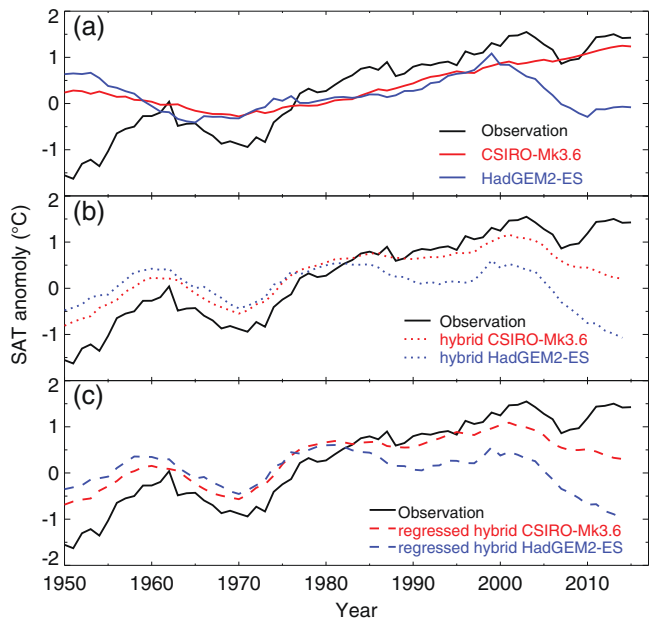


FIGURE 9 Comparison of the time series of the observed SAT based on the 11-year running mean (black) and (a) simulated SAT, (b) “hybrid” SAT in which the simulated DMO component is replaced by the observed DMO, (c) “regressed hybrid” SAT in which the simulated DMO component is replaced by the regressed DMO using PDO, AMO, Niño3.4, and AO climate indexes [Colour figure can be viewed at wileyonlinelibrary.com]

approximately described by the PDO, AMO, Niño3.4, and AO climate indexes. So we also replaced the simulated DMO by the regressed regionally enhanced DMO to “revise” the simulated SAT in the same way, as shown in

Figure 9c. There is a fairly good correspondence between the “regressed hybrid” SAT and “hybrid” SAT.

4 | CONCLUSIONS AND DISCUSSION

In this study, we emphasized the key role of DMO in the decadal signal of climate change. By using the EEMD method to decompose the time series of raw SAT in boreal cold season over the NH land, we defined the sum of IMFs C_3 , C_4 , and C_5 as the DMO, which represents the ICV modulated components of SAT variability on the decadal to multi-decadal scales.

The spatial distribution of DMO trend during warming hiatus revealed two most sensitive regions located in northern Eurasia (Kazakhstan, northwestern Russia, and northeast China) and northwestern North America (western Canada and Alaska), with the DMO fell more than 2°C during 2001–2013. Based on these two most sensitive areas, we extracted the time series of regionally enhanced DMO over the past century. It had a variation at the period of roughly 11–23 years and appeared a gradually intensified oscillation. Regression analysis on regionally enhanced DMO using the PDO, AMO, Niño3.4, and AO illustrated that the DMO over mid-to-high latitudes in NH was primarily dominated by the AO, and the order of contribution to the DMO was the AO (the most), Niño3.4, PDO, and AMO (the least).

The goal of our study on DMO is to shed some light on future climate prediction, so we also investigated the effect of DMO on climate model simulations. There is a huge difference of internal variability between the CMIP5 models and observations over the past 100 years. Furthermore, the extracted regionally enhanced DMO is the key for improving the predictability of SAT over the mid-to-high latitudes of the NH, as our “hybrid” or “regressed hybrid” SAT shows, which points out the direction for future climate model improvement.

ACKNOWLEDGEMENTS

This work was supported by the National Science Foundation of China (41521004, 41722502, 41575006, 91637312) and the China University Research Talents Recruitment Program (111 project, B 13045).

ORCID

Wen Luo  <https://orcid.org/0000-0002-7539-6324>

Xiaodan Guan  <https://orcid.org/0000-0002-5978-7579>

REFERENCES

Bai, L., Xu, J., Chen, Z., Li, W., Liu, Z., Zhao, B. and Wang, Z. (2014) The regional features of temperature variation trends over Xinjiang in China by the ensemble empirical mode decomposition method. *International Journal of Climatology*, 35(11), 3229–3237. <https://doi.org/10.1002/joc.4202>.

Bannister, D., Herzog, M., Graf, H.-F., Hosking, J.S. and Short, C.A. (2017) An assessment of recent and future temperature change over the Sichuan Basin, China, using CMIP5 climate models. *Journal of Climate*, 30(17), 6701–6722. <https://doi.org/10.1175/JCLI-D-16-0536.1>.

Chen, X. and Tung, K.K. (2014) Varying planetary heat sink led to global-warming slowdown and acceleration. *Science*, 345(6199), 897–903. <https://doi.org/10.1126/science.1254937>.

Chen, X. and Tung, K.K. (2016) Correspondence: variations in ocean heat uptake during the surface warming hiatus. *Nature Communications*, 7, 12541. <https://doi.org/10.1038/ncomms12541>.

Chen, Z., Chen, Y., Bai, L. and Xu, J. (2016) Multiscale evolution of surface air temperature in the arid region of northwest China and its linkages to ocean oscillations. *Theoretical and Applied Climatology*, 128(3), 945–958. <https://doi.org/10.1007/s00704-016-1752-7>.

Cohen, J., Screen, J.A., Furtado, J.C., Barlow, M., Whittleston, D., Coumou, D., Francis, J., Dethloff, K., Entekhabi, D., Overland, J. and Jones, J. (2014) Recent Arctic amplification and extreme mid-latitude weather. *Nature Geoscience*, 7(9), 627–637. <https://doi.org/10.1038/Ngeo2234>.

Créat, J., Macron, C., Pohl, B. and Richard, Y. (2011) Quantifying internal variability in a regional climate model: a case study for southern Africa. *Climate Dynamics*, 37(7–8), 1335–1356. <https://doi.org/10.1007/s00382-011-1021-5>.

Créat, J. and Pohl, B. (2012) How physical parameterizations can modulate internal variability in a regional climate model. *Journal of the Atmospheric Sciences*, 69(2), 714–724. <https://doi.org/10.1175/JAS-D-11-0109.1>.

Dai, A., Fyfe, J.C., Xie, S.-P. and Dai, X. (2015) Decadal modulation of global surface temperature by internal climate variability. *Nature Climate Change*, 5(6), 555–559. <https://doi.org/10.1038/nclimate2605>.

Easterling, D.R. and Wehner, M.F. (2009) Is the climate warming or cooling? *Geophysical Research Letters*, 36(8), 262–275. <https://doi.org/10.1029/2009GL037810>.

Fyfe, J.C., Gillett, N.P. and Zwiers, F.W. (2013) Overestimated global warming over the past 20 years. *Nature Climate Change*, 3(9), 767–769. <https://doi.org/10.1038/nclimate1972>.

Fyfe, J.C., Meehl, G.A., England, M.H., Mann, M.E., Santer, B.D., Flato, G.M., Hawkins, E., Gillett, N.P., Xie, S.P., Kosaka, Y. and Swart, N.C. (2016) Making sense of the early-2000s warming slowdown. *Nature Climate Change*, 6(3), 224–228. <https://doi.org/10.1038/nclimate2938>.

Gong, D.Y. and Ho, C.H. (2003) Arctic Oscillation signals in the East Asian summer monsoon. *Journal of Geophysical Research*, 108(D2), 4066. <https://doi.org/10.1029/2002JD002193>.

Gong, D.Y. and Wang, S.W. (2003) Influence of Arctic Oscillation on winter climate over China. *Journal of Geographical Sciences*, 13 (2), 208–216. <https://doi.org/10.1007/bf02837460>.

Gong, D.Y., Wang, S.W. and Zhu, J.H. (2001) East Asian winter monsoon and Arctic Oscillation. *Geophysical Research Letters*, 28(10), 2073–2076. <https://doi.org/10.1029/2000GL012311>.

Guan, X., Huang, J. and Guo, R. (2017) Changes in aridity in response to the global warming hiatus. *Journal of Meteorological Research*, 31(1), 117–125. <https://doi.org/10.1007/s13351-017-6038-1>.

Guan, X., Huang, J., Guo, R. and Lin, P. (2015a) The role of dynamically induced variability in the recent warming trend slowdown over the Northern Hemisphere. *Science Report*, 5, 12669. <https://doi.org/10.1038/srep12669>.

Guan, X., Huang, J., Guo, R., Yu, H., Lin, P. and Zhang, Y. (2015b) Role of radiatively forced temperature changes in enhanced semi-arid warming in the cold season over East Asia. *Atmospheric Chemistry and Physics*, 15(23), 13777–13786. <https://doi.org/10.5194/acp-15-13777-2015>.

Hansen, J., Sato, M., Ruedy, R., Lo, K., Lea, D.W. and Medina-Elizade, M. (2006) Global temperature change. *Proceedings of the National Academy of Sciences of the United States of America*, 103 (39), 14288–14293. <https://doi.org/10.1073/pnas.0606291103>.

Harris, I., Jones, P.D., Osborn, T.J. and Lister, D.H. (2014) Updated high-resolution grids of monthly climatic observations—the CRU TS3.10 dataset. *International Journal of Climatology*, 34(3), 623–642. <https://doi.org/10.1002/joc.3711>.

Higuchi, K., Huang, J. and Shabbar, A. (1999) A wavelet characterization of the North Atlantic Oscillation variation and its relationship to the North Atlantic sea surface temperature. *International Journal of Climatology*, 19(10), 1119–1129. [https://doi.org/10.1002/\(SICI\)1097-0088\(199908\)19:10<1119::AID-JOC414>3.0.CO;2-7](https://doi.org/10.1002/(SICI)1097-0088(199908)19:10<1119::AID-JOC414>3.0.CO;2-7).

Holland, M.M. and Bitz, C.M. (2003) Polar amplification of climate change in coupled models. *Climate Dynamics*, 21(3–4), 221–232. <https://doi.org/10.1007/s00382-003-0332-6>.

Hopsch, S., Cohen, J. and Dethloff, K. (2012) Analysis of a link between fall Arctic sea ice concentration and atmospheric patterns in the following winter. *Tellus A: Dynamic Meteorology and Oceanography*, 64(1), 18624. <https://doi.org/10.3402/tellusa.v64i0.18624>.

Huang, B. and Liu, Z. (2000) Temperature trend of the last 40 yr in the upper pacific ocean. *Journal of Climate*, 14(17), 3738–3750. [https://doi.org/10.1175/1520-0442\(2001\)014<3738:TTOTLY>2.0.CO;2](https://doi.org/10.1175/1520-0442(2001)014<3738:TTOTLY>2.0.CO;2).

Huang, J., Ji, M., Higuchi, K. and Shabbar, A. (2006) Temporal structures of the North Atlantic Oscillation and its impact on the regional climate variability. *Advances in Atmospheric Sciences*, 23(1), 23–32. <https://doi.org/10.1007/s00376-006-0003-8>.

Huang, J., Xie, Y., Guan, X., Li, D. and Ji, F. (2016) The dynamics of the warming hiatus over the Northern Hemisphere. *Climate Dynamics*, 48(1–2), 429–446. <https://doi.org/10.1007/s00382-016-3085-8>.

Huang, N.E., Shen, Z., Long, S.R., Wu, M.C., Shih, H.H., Zhang, Q., Yen, N.C., Tung, C.C. and Liu, H.H. (1998) The empirical mode decomposition and the Hilbert spectrum for nonlinear and non-stationary time series analysis. *Proceedings Mathematical Physical & Engineering Sciences*, 454(1971), 903–995. <https://doi.org/10.1098/rspa.1998.0193>.

Ji, F., Wu, Z., Huang, J. and Chassignet, E.P. (2014) Evolution of land surface air temperature trend. *Nature Climate Change*, 4(6), 462–466. <https://doi.org/10.1038/nclimate2223>.

Kaufmann, R.K., Kauppi, H., Mann, M.L. and Stock, J.H. (2011) Reconciling anthropogenic climate change with observed temperature 1998–2008. *Proceedings of the National Academy of Sciences of the United States of America*, 108(29), 11790–11793. <https://doi.org/10.1073/pnas.1102467108>.

Kosaka, Y. and Xie, S. (2013) Recent global-warming hiatus tied to equatorial Pacific surface cooling. *Nature*, 501(7467), 403–407. <https://doi.org/10.1038/nature12534>.

L'Heureux, M.L., Lee, S. and Lyon, B. (2013) Recent multidecadal strengthening of the Walker circulation across the tropical Pacific. *Nature Climate Change*, 3(6), 571–576. <https://doi.org/10.1038/NCLIMATE1840>.

Li, B., Chen, Y. and Shi, X. (2012) Why does the temperature rise faster in the arid region of northwest China? *Journal of Geophysical Research: Atmospheres*, 117, D16115. <https://doi.org/10.1029/2012JD017953>.

Li, Q., Yang, S., Xu, W., Wang, X.L., Jones, P., Parker, D., Zhou, L., Feng, Y. and Gao, Y. (2015) China experiencing the recent warming hiatus. *Geophysical Research Letters*, 42(3), 889–898. <https://doi.org/10.1002/2014GL062773>.

Li, Q.J., Zhao, Y., Liao, H.L. and Li, J.K. (2017) Effective forecast of Northeast Pacific sea surface temperature based on a complementary ensemble empirical mode decomposition–support vector machine method. *Atmospheric and Oceanic Science Letters*, 10(3), 261–267. <https://doi.org/10.1080/16742834.2017.1305867>.

Liu, B. and Zhou, T. (2017) Atmospheric footprint of the recent warming slowdown. *Scientific Reports*, 7, 40947. <https://doi.org/10.1038/srep40947>.

Luo, D., Yao, Y., Dai, A. and Feldstein, S.B. (2015) The positive North Atlantic Oscillation with downstream blocking and Middle East snowstorms: the large-scale environment. *Journal of Climate*, 28 (16), 6398–6418. <https://doi.org/10.1175/JCLI-D-15-0184.1>.

Mao, R., Gong, D.Y., Yang, J. and Bao, J.D. (2011) Linkage between the Arctic Oscillation and winter extreme precipitation over central-southern China. *Climate Research*, 50, 187–201. <https://doi.org/10.3354/cr01041>.

Meehl, G.A., Hu, A., Santer, B.D. and Xie, S.P. (2016) Contribution of the Interdecadal Pacific Oscillation to twentieth-century global surface temperature trends. *Nature Climate Change*, 6(11), 1005–1008. <https://doi.org/10.1038/nclimate3107>.

Meinshausen, M., Smith, S.J., Calvin, K., Daniel, J.S., Kainuma, M.L., T., Lamarque, J.F., Matsumoto, K., Montzka, S.A., Raper, S.C.B., Riahi, K., Thomson, A., Velders, G.J.M. and Vuuren van D.P.P. (2011) The RCP greenhouse gas concentrations and their extensions from 1765 to 2300. *Climatic Change*, 109, 213–241. <https://doi.org/10.1007/s10584-011-0156-z>.

Overland, J.E. and Wang, M. (2010) Large-scale atmospheric circulation changes are associated with the recent loss of Arctic sea ice. *Tellus A: Dynamic Meteorology and Oceanography*, 62(1), 1–9. <https://doi.org/10.1111/j.1600-0870.2009.00421.x>.

Qian, C., Fu, C., Wu, Z. and Yan, Z. (2009) On the secular change of spring onset at Stockholm. *Geophysical Research Letters*, 36(12), L12706. <https://doi.org/10.1029/2009GL038617>.

Qian, C., Fu, C., Wu, Z. and Yan, Z. (2011a) The role of changes in the annual cycle in earlier onset of climatic spring in northern China. *Advances in Atmospheric Sciences*, 28(2), 284–296. <https://doi.org/10.1007/s00376-010-9221-1>.

Qian, C., Wu, Z., Fu, C. and Wang, D. (2011b) On changing El Niño: a view from time-varying annual cycle, interannual variability and mean state. *Journal of Climate*, 24, 6486–6500. <https://doi.org/10.1175/jcli-d-10-05012.1>.

Serreze, M.C., Barrett, A.P., Stroeve, J.C., Kindig, D.M. and Holland, M.M. (2009) The emergence of surface-based Arctic

amplification. *Cryosphere*, 3(1), 11–19. <https://doi.org/10.5194/tc-3-11-2009>.

Shan, H., Guan, Y., Huang, J. and Dong, C. (2017) Trajectory patterns of the annual cycle of the heat centre of the Indo-Pacific warm pool. *International Journal of Climatology*, 37(2), 637–647. <https://doi.org/10.1002/joc.4729>.

Smoliak, B.V., Wallace, J.M., Lin, P. and Fu, Q. (2015) Dynamical adjustment of the Northern Hemisphere surface air temperature field: methodology and application to observations. *Journal of Climate*, 28 (4), 1613–1629. <https://doi.org/10.1175/JCLI-D-14-00111.1>.

Steinman, B.A., Mann, M.E. and Miller, S.K. (2015) Atlantic and Pacific Multidecadal Oscillations and Northern Hemisphere temperatures. *Science*, 347(6225), 988–991. <https://doi.org/10.1126/science.1257856>.

Stocker, T.F., Qin, D., Plattner, G.K., Tignor, M., Allen, S.K., Boschung, J., Nauels, A., Xia, Y., Bex, V. and Midgley, P.M. (eds.) (2013) IPCC: summary for policymakers. In: *Climate Change 2013: The Physical Science Basis*. Cambridge, UK and New York, NY: Cambridge University Press.

Taylor, K.E., Stouffer, R.J. and Meehl, G.A. (2011) An overview of CMIP5 and the experiment design. *Bulletin of the American Meteorological Society*, 93(4), 485–498. <https://doi.org/10.1175/BAMS-D-11-00094.1>.

Thompson, D.W.J. and Wallace, J.M. (1998) The Arctic Oscillation signature in the wintertime geopotential height and temperature fields. *Geophysical Research Letters*, 25(9), 1297–1300. <https://doi.org/10.1029/98GL00950>.

Thompson, D.W.J. and Wallace, J.M. (2001) Regional climate impacts of the Northern Hemisphere annular mode. *Science*, 293(5527), 85–89. <https://doi.org/10.1126/science.1058958>.

Tung, K. and Zhou, J. (2013) Using data to attribute episodes of warming and cooling in instrumental records. *Proceedings of the National Academy of Sciences of the United States of America*, 110 (6), 2058–2063. <https://doi.org/10.1073/pnas.1212471110>.

Wallace, J.M., Fu, Q., Smoliak, B.V., Lin, P. and Johanson, C.M. (2012) Simulated versus observed patterns of warming over the extratropical Northern Hemisphere continents during the cold season. *Proceedings of the National Academy of Sciences of the United States of America*, 109(36), 14337–14342. <https://doi.org/10.1073/pnas.1204875109>.

Wettstein, J.J. and Mearns, L.O. (2002) The influence of the North Atlantic–Arctic Oscillation on mean variance and extremes of temperature in the northeastern United States and Canada. *Journal of Climate*, 15(24), 3586–3600. [https://doi.org/10.1175/1520-0442\(2002\)0152.0.CO;2](https://doi.org/10.1175/1520-0442(2002)0152.0.CO;2).

Wu, B.Y. and Wang, J. (2002) Winter Arctic Oscillation, Siberian High and East Asian winter monsoon. *Geophysical Research Letters*, 29 (19), 1897. <https://doi.org/10.1029/2002GL015373>.

Wu, Z. and Huang, N.E. (2009) Ensemble empirical mode decomposition: a noise assisted data analysis method. *Advances in Adaptive Data Analysis*, 1(01), 1–41. <https://doi.org/10.1142/S1793536909000047>.

Wu, Z., Huang, N.E., Long, S.R. and Peng, C.K. (2007) On the trend, detrending, and variability of nonlinear and nonstationary time series. *Proceedings of the National Academy of Sciences of the United States of America*, 104(38), 14889–14894. <https://doi.org/10.1073/pnas.0701020104>.

Wu, Z., Huang, N.E., Wallace, J.M., Smoliak, B.V. and Chen, X. (2011) On the time-varying trend in global-mean surface temperature. *Climate Dynamics*, 37(3–4), 759–773. <https://doi.org/10.1007/s00382-011-1128-8>.

Wyatt, M.G., Kravtsov, S. and Tsonis, A.A. (2012) Atlantic multidecadal Oscillation and Northern Hemisphere's climate variability. *Climate Dynamics*, 38(5), 929–949. <https://doi.org/10.1007/s00382-011-1071-8>.

Xie, Y., Huang, J. and Liu, Y. (2017) From accelerated warming to warming hiatus in China. *International Journal of Climatology*, 37 (4), 1758–1773. <https://doi.org/10.1002/joc.4809>.

Xu, C.H. and Xu, Y. (2012) The projection of temperature and precipitation over China under RCP scenarios using a CMIP5 multi-model ensemble. *Atmospheric and Oceanic Science Letters*, 5(6), 527–533. <https://doi.org/10.1080/16742834.2012.11447042>.

Zhang, H., Qin, J. and Li, Y. (2011) Climatic background of cold and wet winter in southern China: part I observational analysis. *Climate Dynamics*, 37(11–12), 2335–2354. <https://doi.org/10.1007/s00382-011-1022-4>.

Zhang, Y. (2012) Projections of 2.0°C warming over the globe and China under RCP4.5. *Atmospheric and Oceanic Science Letters*, 5 (6), 514–520. <https://doi.org/10.1080/16742834.2012.11447047>.

Zhang, Y., Guan, X., Yu, H., Xie, Y. and Jin, H. (2017) Contributions of radiative factors to enhanced dryland warming over East Asia. *Journal of Geophysical Research Atmospheres*, 122, 7723–7736. <https://doi.org/10.1002/2017JD026506>.

Zhang, Z.Y., Wong, M.S. and Nichol, J. (2016) Global trends of aerosol optical thickness using the ensemble empirical mode decomposition method. *International Journal of Climatology*, 36(13), 4358–4372. <https://doi.org/10.1002/joc.4637>.

How to cite this article: Luo W, Guan X, Xie Y, Liu J, Zhou Y, Zhang B. The key role of decadal modulated oscillation in recent cold phase. *Int J Climatol*. 2019;1–10. <https://doi.org/10.1002/joc.6186>